AIAA JOURNAL
Vol. 32, No. 7, July 1994

Planar Air Density Measurements near Model Surfaces by Ultraviolet Rayleigh/Raman Scattering

G. Grünefeld* and V. Beushausen†
Laser-Laboratorium Göttingen, D-37077 Göttingen, Germany
and
P. Andresen‡
University of Bielefeld, D-33615 Bielefeld, Germany

The feasibility of planar ultraviolet laser-induced Rayleigh and Raman scattering for measurements of small air density variations near model wing surfaces is tested for applications in wind tunnels. Variations in air density of less than 1% are measured quantitatively by Rayleigh scattering in a plane of 3×6 cm^2 in about 1 s under the extreme condition in which the laser directly irradiates the metal surface of the wing. Raman scattering was tested as well because it is much less affected by surface and Mie scattering. Therefore, it can be used for density measurements much closer to the model surface and under the presence of dust and droplets with a precision of at least 2%. Further improvements of the measurement precision are possible and will be discussed.

Introduction

QUANTITATIVE density and temperature measurements in air are very important in aerodynamical and other applications. Shock structures occurring across the wings of aircraft, and small density differences close to metallic surfaces of turbine blades are just two examples. For such measurements, nonintrusive laser diagnostic methods are desired. However, very few laser diagnostic methods appear to be useful for highly precise measurements in pure air. Those that are include Rayleigh scattering,[1-3] spontaneous Raman scattering, and laser-induced fluorescence (LIF). Whereas Rayleigh and Raman scattering can be performed, in principle, at every excitation wavelength, LIF is only possible with oxygen via the Schumann Runge bands in the deep uv.[4] Until now, no quantitative LIF method has been found for nitrogen.

The most promising lasers for highly precise measurements using Rayleigh and Raman scattering are deep uv lasers, such as excimer lasers or frequency quadrupled Nd:YAG lasers, which are the most powerful commercially available lasers in the deep uv. Both Rayleigh and Raman scattering intensities become very strong in the deep uv because their cross sections increase with the fourth power of frequency.[1,2] The Raman scattering cross section of air at 193 nm (ArF laser) is roughly 100 times higher than it is at 532 nm (Ref. 5), where frequency doubled Nd:YAG lasers have been applied extensively for Rayleigh and Raman scattering.[3,6] Because the number of photons per pulse is somewhat higher in commercially available Nd:YAG than in excimer lasers, excimer lasers yield an increase in scattering intensity of roughly 50. Tunable excimer lasers can be used additionally for the laser-induced predissociation fluorescence (LIPF) of oxygen.

The scaling of the cross section with the fourth power of frequency yields another advantage. The precision of both Rayleigh and Raman density measurements is, in almost all cases, limited by scattered light from windows, surfaces, and particles because appropriate filters are not yet available for deep uv wavelengths (Miles and Lempert[6] developed a Mie filter for 532 nm). Both Mie and surface-scattering cross sections become geometrical for larger particles and are consequently roughly independent of frequency (absorption is also usually stronger in the uv). The contrast is therefore increased by roughly a factor of 50 when applying a short-wavelength excimer as compared to Nd:YAG lasers at 532 nm. The most promising laser sources for Raman and Rayleigh scattering are therefore the KrF (248 nm) or the ArF (193 nm) laser, because they yield the largest scattering intensities. In some cases, where the interference with Mie and surface scattering is more severe, ArF lasers may be preferred.

In the experiments described in this paper, tunable ArF and KrF excimer lasers were used to analyze the precision of planar air density measurements in close proximity to a model of an aircraft wing. Both Rayleigh scattering (at 193 and 248 nm) and Raman scattering (at 248 nm) were tested for this purpose. These experiments were conducted for future application of this technique in the European Transonic Windtunnel (Cologne, Germany), where shock structures near model wings shall be made visible. It was one major aim of this work to reduce the measurement time as much as possible.

Experimental

The experimental setup is shown in Fig. 1. The light of a tunable excimer laser (1) was formed to a sheet (30-mm height). A plate of birefringent MgF_2 (8) was used to rotate the electric vector of the laser radiation by tilting the plate to different angles with respect to the beam. The laser light sheet was directed towards the aluminium wing model (2), which could be tilted via the angles c and ℓ

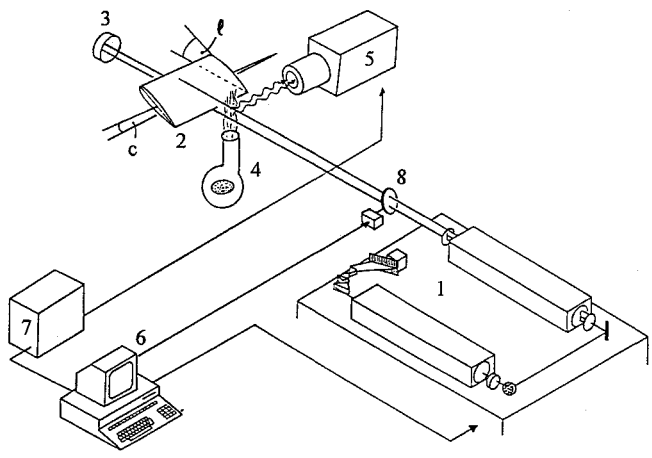

Fig. 1 Experimental setup.

Received Sept. 2, 1993; revision received Jan. 4, 1994; accepted for publication Jan. 7, 1994.

*Graduate Student, Hans-Adolf-Krebs Weg 1.
†Doctor Scientist, Hans-Adolf-Krebs Weg 1.
‡Professor, Universitätsstrasse 25.

relative to the camera axis and laser beam, respectively. The remaining laser light is trapped in a beam stop (3). The emitted Rayleigh and Raman light is imaged via a lens with rather poor collection efficiency (uv Nikkor 105 mm, f4.5) at right angles to an intensified charge-coupled device (CCD) camera (La Vision). The distance between the laser beam and the front end of the objective was 50 cm so that an area of 47×63 mm was imaged onto the CCD chip. The spatial resolution of the imaging system was determined to be about 0.3 mm, corresponding to three pixels.

A fan (4), mounted in close proximity to the surface of the wing, was used to generate a small and well-known density difference by heating the room air around the wing to slightly higher temperatures. The air temperature was measured with a thermocouple turning the fan off (T_0, ρ_0) and on (T, ρ). According to the ideal gas law at constant pressure, the density is varied by a known fraction f

$$f=(\rho_0-\rho)/\rho=(T-T_0)/T_0$$

This setup allowed a simple way to determine the distance from the surface where the small density differences introduced by the fan could still be seen in the corresponding Rayleigh and Raman images.

The angles of the wing relative to the laser beam and camera axis were varied in the experiment, because the amount of stray light, and consequently the measurement precision, depended strongly on the orientation of the scattering source relative to the laser and the camera.

The excimer laser (1) used was a tunable narrowband EMG 160 MSC (Lambda-Physik). It consists of an oscillator and an amplifier part. This is not described in detail here as narrow bandwidth and tunability was not necessary for these experiments. The pulse length was about 25 ns and the typical repetition rates were 50–100 Hz. The laser was operated on ArF generating about 100 mJ per pulse at 193 nm for most of the Rayleigh scattering experiments. For comparison of the results with another wavelength, a similar KrF laser was used as well (248 nm, 150 mJ per pulse).

The radiation generated by these lasers is almost linearly polarized so that signal enhancement could be achieved by adjusting the best orientation of the E vector with regard to the detector. This was done by the rotatable MgF_2 plate (8) in the laser beam as was mentioned earlier. This also offers the possibility of distinguishing between Rayleigh (or Raman) scattering and other emissions that are independent of the E-vector direction. The most important example of such an interfering emission in this application is the intense stray light from the model wing surface. (In fact, the observed signal intensity of light scattered by the model surface turned out to be independent of the E-vector direction, in contrast to Rayleigh scattering, see following.)

An AT personal computer (6) controlled the whole experiment, i.e., it triggered the laser and the camera system via a timing unit (7), adjusted the MgF_2 plate by a stepper motor, and acquired the CCD images.

Because the integration time of the CCD camera is variable, it was possible to integrate up to several hundred laser pulses on-chip.

The setup for the spontaneous Raman scattering experiments was nearly the same as that for the Rayleigh scattering measurements with the exception of careful filtering. Two types of filters were placed in front of the camera system to discriminate the vibrational Stokes Raman bands of the room air components (N_2, O_2, and H_2O) against interfering emissions. The first filter efficiently absorbed the laser wavelength itself, and the second suppressed all wavelengths longer than 290 nm, which is beyond the vibrational Raman bands for air. The second filter was necessary to avoid the collection of broadband laser-induced fluorescence from dust (especially hydrocarbons) in the air and on the model wing. In these experiments the 248-nm laser was used for two reasons: 1) the broadband laser-induced fluorescence appears to a much smaller degree compared with 193 nm, and 2) a filter (liquid butyl acetate) was available which absorbed the laser wavelength very efficiently and transmitted the Stokes Raman wavelengths relatively freely (recent results of McKenzie[7] show that a simple acetone/water mixture can be used as a filter for 193-nm radiation as well). A 25-mm-thick layer of butyl acetate suppressed the 248-nm light by eight orders of magnitude, so that the remaining Rayleigh scattering contribution was negligible. The nearest vibrational Raman band (of oxygen at 258 nm) was only attenuated by about 25% (and the nitrogen band at 263.5 nm less than 10%). This liquid filter was also sufficient to completely suppress Mie scattering and to effectively attenuate the stray light from the metallic surface. For suppression of the longer wavelengths two dielectric laser mirrors coated for 248 nm (45 deg) were used under

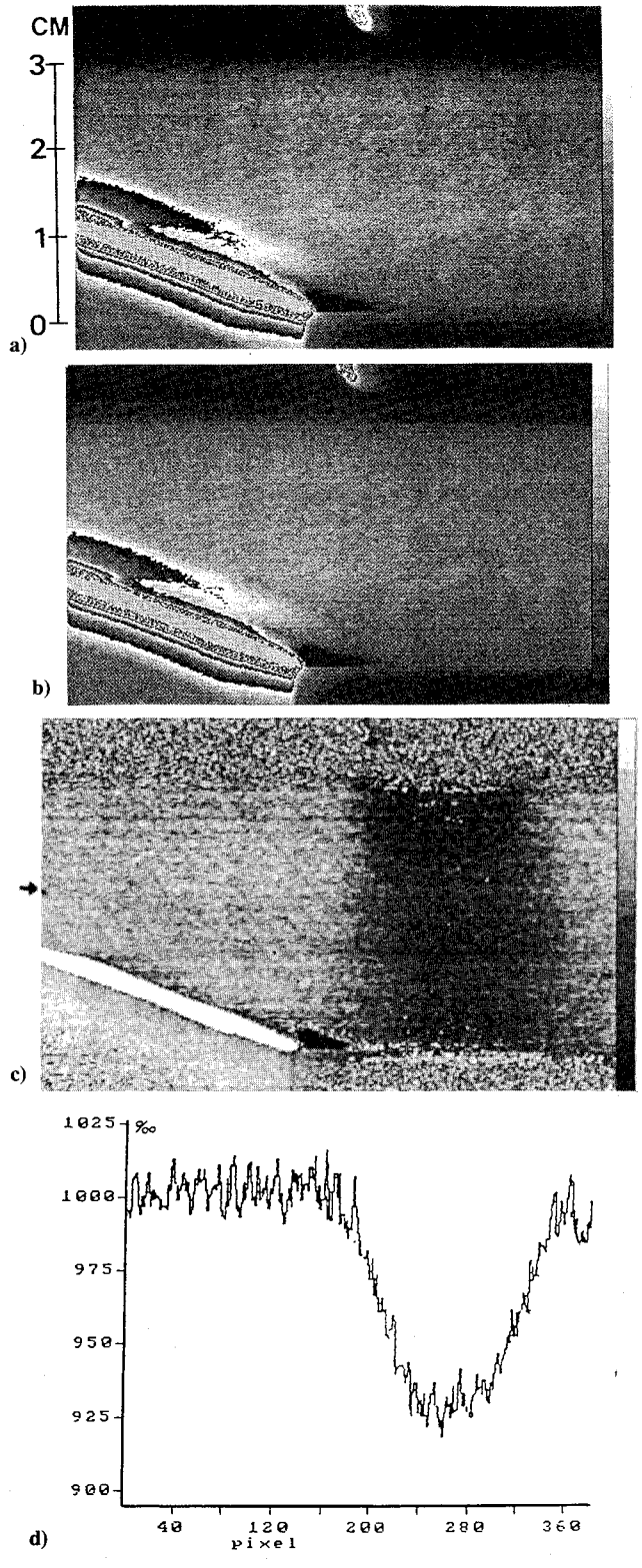

Fig. 2 Raw images with a) the fan turned on, and b) off; c) the calibrated result from division of a) and b); and d) horizontal profile from c) averaged over three rows indicated by the arrow.

an angle of incidence of 35 deg. This resulted in high transmission between 250 and 280 nm and an attenuation of over 90% for wavelengths longer than about 300 nm.

For the first Raman imaging experiments the unfocused laser beam with a height of 30 mm was used in a fashion similar to that in the Rayleigh scattering experiments at 248 nm (the imaging scale was not changed by the filtering optics). In other experiments, the height of the laser beam was reduced by a factor of 2.4 using a spherical lens ($f = 2$ m) to achieve a higher signal level.

Results of the Rayleigh Scattering Experiments

The images in Fig. 2 are shown to explain the measurement procedure. Both images, Figs. 2a and 2b, are the emission from 40 laser shots (the conversion of intensities to gray levels is indicated by the gray scale at the right sides of the images). The largest density variation is $(\rho_0-\rho)/\rho = 0.076$, i.e., 7.6%, as deduced from the maximum temperature observed with the thermocouple [$T_0 = 295$ K, $T_1 = 317$ K, $(T-T_0) = 22$ K].

A raw image $S_1(x, y)$, with the fan turned on, is shown in Fig. 2a. The emission which is by far the strongest in the image results from surface scattering and not from the air. The most intense emission, where the dynamic range of the camera is saturated, originates, as expected, from the section of the surface of the wing that is directly irradiated by the laser (left side, below). (In this case the fan is positioned above, in contrast to the drawing in Fig. 1, so that some intense stray light from the fan nozzle is also seen in the upper middle of Fig. 2a.) The Rayleigh scattering from air shows up in the middle at the right side of the wing. The intensity distribution is very inhomogeneous because of the laser beam inhomogeneities and the spatially dependent sensitivity of the imaging optics. The density variation introduced by the fan cannot be seen in this image because it is much smaller than these aberrations. To see the density variation introduced by the fan a second image is recorded with the fan turned off under otherwise identical conditions yielding, the image $S_0(x, y)$ in Fig. 2b. Figure 2b has such a close similarity to Fig. 2a that one might not dare to say whether there is a density difference at all.

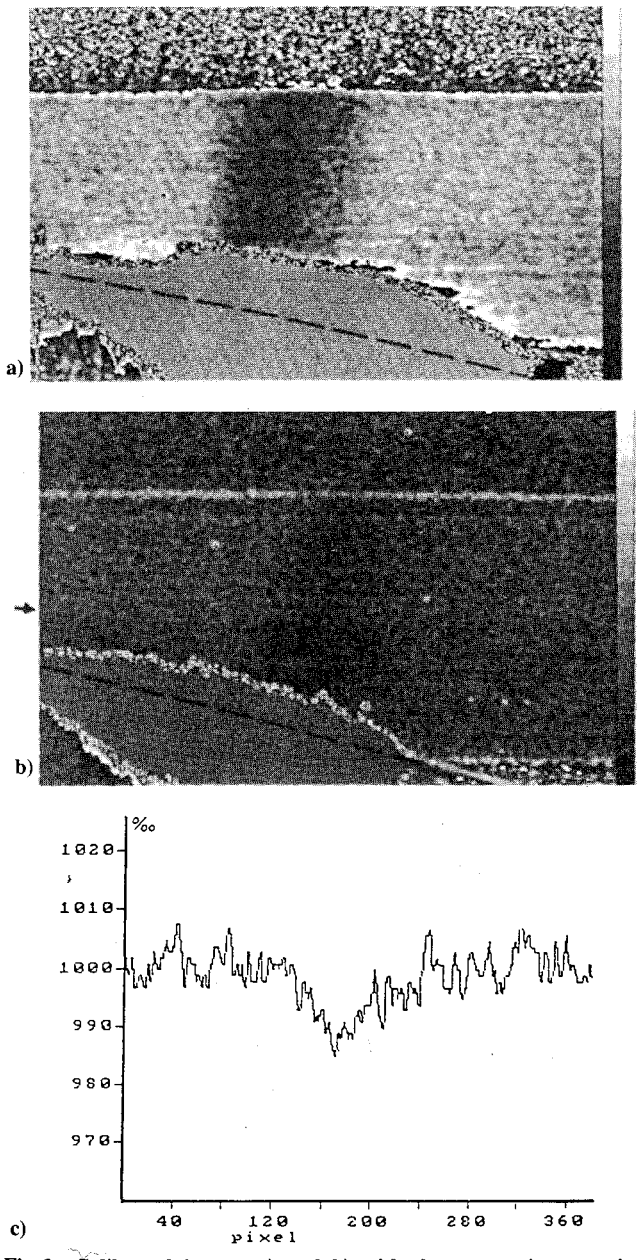

Fig. 3 Calibrated images a) and b) with the warm air streaming upwards through a slit in the wing; both images were averaged over nine neighboring pixels after division of the raw images; and c) horizontal profile from b) averaged over three rows at the position of the arrow.

The density variation shows up only after appropriate image processing, i.e., if the two images are divided by each other (i.e., the intensity S_1 is divided by the intensity S_0 at the same pixel). This division yields image Fig. 2c. The measured signal $S_i(x, y)$ is related to the true density $\rho_i(x, y)$ via the spatially dependent sensitivity $E(x, y)$, which depends on all of the aforementioned features of the optical setup, but it is constant for a given setup:

$$S_i(x, y) = E(x, y)\rho_i(x, y)$$

The spatially dependent sensitivity cancels out, if the signals are divided:

$$S_1(x, y)/S_0(x, y) = [E(x, y)\rho_1(x, y)]/[E(x, y)\rho_0(x, y)]$$

$$= \rho_1(x, y)/\rho_0(x, y)$$

It should be noted that the identical optical setup has to be used in both measurements, because $E(x, y)$ does not stay the same if it is not.

Across the field of view we obtain the unknown density:

$$\rho_1(x, y) = S_1(x, y)/S_0(x, y)\rho_0(x, y)$$

Because $\rho_0(x, y)$ is known from measurements of p_0 and T_0 for room air, the absolute density is easily calculated.

Now the density difference introduced by the fan is clearly seen: the density is considerably reduced at the spatial position of the warm air stream. The density gradients to the sides are also seen in the image. For quantitative analysis, a horizontal profile is shown below (Fig. 2d). This profile is averaged over three pixel rows indicated by an arrow on the left side of Fig. 2c. The profile varies from 900 to 1025, i.e., the variation from 1000 to 925 corresponds to a density variation of 7.5%. The maximum observed density difference agrees very well with the thermocouple measurement (7.6%). The noise along the horizontal profile is roughly 15, i.e., the density difference of 7.5% is measured with a signal-to-noise ratio (S/N) of 5. This implies that a density difference of 1.5% is measured with a S/N of 1. It should be emphasized here that the 40 laser shots are recorded in less than a second.

It should also be mentioned that the division of the images yields not only absolute densities but also eliminates many potential sources of errors and contains an implicit calibration. In principle, large variations in spatially dependent sensitivity are expected from the optical setup because different solid angles are sampled from different parts of the image, because the gain is pixel dependent, and because inhomogeneities in the laser beam profile, etc. occur which make a quantification of images such as Fig. 2a or 2b alone almost impossible.

It is important to note that the easy calibration procedure just described works only in the observed areas which are unaffected by scattered light from surfaces: if $S(x, y)$ is not the pure Rayleigh signal, as is the case near the model wing surface, it is no longer proportional to the density $n(x, y)$. Thus underlying stray light from the surface results in distortion of the density scale if the discussed

calibration procedure is applied. However, density variations can still be observed, at least qualitatively, even if large amounts of surface scattered light are present, if this stays unchanged when the calibration image in homogeneous air is recorded.

Quantitative detection of small density differences, even in the presence of high quantities of surface scattered light, i.e., close to the model wing, is possible by an alternative calibration procedure. For this purpose an additional calibration image would have to be recorded with the same setup but with the Rayleigh scattering strongly suppressed. This could be achieved with a parallel adjustment of the E vector of laser light to the camera axis. Because the surface scattering intensity is independent of the E-vector direction, as verified in the experiment, the pure Rayleigh scattering signal could be calculated from images such as Figs. 2a and 2b using this additional calibration image. (For this purpose the suppression factor of Rayleigh scattering must be determined and taken into account.) The two resulting images (surface-scattered light subtracted) could be divided, which would yield quantitative density variations.

To determine whether small density differences can still be measured if the laser hits directly the surface of the model wing, a portion of the warm air stream from the fan was directed through a slit in the wing. The image in Fig. 3a results from the division of an image acquired with the fan turned on (150 laser shots) and a calibration image with the fan turned off (300 laser shots). The exact position of the model wing surface, where it was hit by the laser beam, is indicated in the image by a line (as it was observed by single shot illumination of the surface). This line is surrounded by an area of very intense surface scattering, where the CCD chip was saturated, resulting in a large, single-colored area. A second neighboring area can be seen, where the CCD chip was not saturated, but large amounts of surface-scattered light were present. This is seen because the measured density difference is smaller than in the undisturbed region higher above the wing. However, only a zone of about 10 mm above the model wing is affected by surface scattering. Because this zone has, for the most part, saturated on the CCD chip, it could not be corrected using the technique of E-vector rotation. (The extension of the saturated area could be reduced by integrating fewer laser shots on-chip and, instead of this, adding several camera images after acquisition. On the other hand, this would result in longer measurement times because more than one camera read out would be necessary, which was not the aim of the present experiments.)

The extension of the saturated area near the model wing position depends strongly on the angles ℓ and c of the surface with regard to the laser beam direction and camera axis, respectively. For Fig. 3 the angle ℓ was 16 deg ($c = 0$ deg). For example, if the angle ℓ is reduced to 8 deg ($c = 0$ deg) under the same conditions, the saturated area decreases to about 2 mm above the surface. In this situation the warm air flow could be observed quantitatively a few millimeters above the wing because the surface scattering intensity strongly decreased with growing distance from the surface.

Because the intensity of surface-scattered light is a measure for the extension of the area where pixel overflow occurs, this intensity was detected quantitatively in different situations. It turned out that the intensity depends more strongly on the angle c of the surface (with regard to the camera) than on the angle ℓ. For example, for $c = 2.5$ deg the maximum ratio of light scattered by the surface to pure Rayleigh scattering in the air S/R was about:

$$S/R(\ell = 5 \text{ deg}) = 30$$

$$S/R(\ell = 10 \text{ deg}) = 100$$

$$S/R(\ell = 20 \text{ deg}) = 420$$

For fixed $\ell = 10$ deg and different c values the ratio was roughly:

$$S/R(c = 0 \text{ deg}) = 25$$

$$S/R(c = 5 \text{ deg}) = 400$$

Further increase of the angle c was avoided because the S/R ratio increased dramatically.

The experiment showed that these ratios also depend on the roughness of the metallic surface. To demonstrate this effect the polished front part of the model wing was illuminated by the laser beam. Here the S/R ratios were approximately halved. (The polished surface allowed to measure with an angle ℓ of nearly 90 deg at the front end of the model wing.) This situation is shown in Fig. 4 where c was again about 0 deg. The laser was directed from the left to the right in these measurements, in contrast to Figs. 2 and 3. Again the model surface is indicated by a line. The decrease of surface scattering intensity with decreasing angle of incidence ℓ can be estimated in the region of the leading edge. It can be seen in Fig. 4a that the saturated region extends roughly 3 mm (on average) above the wing surface. An additional 7 mm are affected by light scattered from the surface. (Above the laser sheet some light scattered by materials in the background can be seen.) For quantitative measurements in this area the technique of E-vector rotation could be used.

Figure 4b shows the calibrated result from Fig. 4a using 150 laser shots with the fan turned off for reference image. In the left half of the figure, directly in front of the wing, the warm air from the blower can be seen streaming upwards.

The precision of density measurements is essentially limited by photoelectron statistics, i.e., by the number of photoelectrons N generated at the photocathode of the image intensifier of the CCD camera corresponding to one pixel. According to Poisson statistics, the relative uncertainty in the measured value for the density is $1/N^{1/2}$ for N photoelectrons. The number of photoelectrons can be increased in various ways to reduce the measurement uncertainty and to achieve higher precision. These include larger collection solid angle of imaging optics, summing up over more laser shots, and summing up—at the cost of spatial resolution—the signal from neighboring pixels.

To demonstrate that the precision is indeed determined by photoelectron statistics (up to a certain limit), and that higher measurement precision is achieved, a smaller density variation was generated by reducing the temperature of the fan. For the image shown in Fig. 3b the maximum density variation was set to about 1% [maximum $(T - T_0) = 3$ K]. The 300 laser shots were summed up

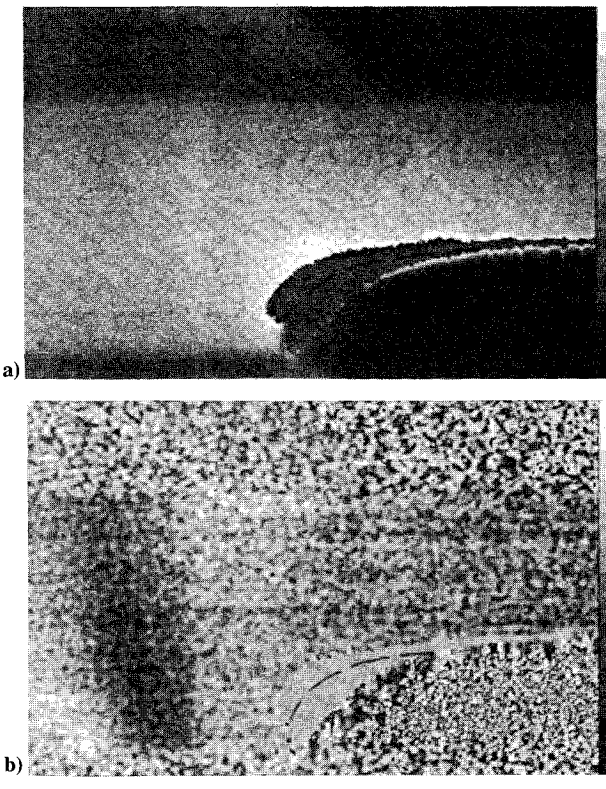

Fig. 4 Raw image a) with the laser sheet illuminating the round front end of the model wing; b) is the calibrated result of a).

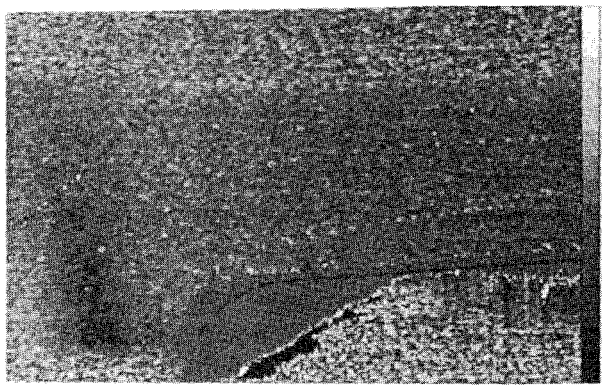

Fig. 5 Calibrated image from Rayleigh scattering at 248 nm; some spots from Mie scattering can be seen at the left side, at the upper right side, and near the model surface.

for both measurement and calibration images. Moreover, Fig. 3a (and 3b) was generated by averaging over nine neighboring pixels, i.e., each pixel value is the average of its original value and its eight nearest neighbors. This procedure does not result in great loss of spatial resolution, which was in the region of three pixels anyway.

As a result, the warm air stream with a maximum occurring density difference of 0.9% can be seen clearly. This would not be possible with 40 laser shots as discussed earlier (Fig. 2). To quantify the measurement precision a horizontal profile (averaged over three pixel rows indicated by an arrow on the left side of Fig. 3b) is given in Fig. 3c. The y scale extends from 960 to 1020, i.e., over 6% of the total density. The dip in the profile goes down to 990, corresponding to a density variation of 1% as was expected from the thermocouple measurement.

It is known from an earlier calibration of the camera system how the number of photoelectrons generated in the photocathode is related to the number of counts. Thus, the expected standard deviation of neighboring pixels in an area of Rayleigh scattering from homogeneous room air in the images can be calculated from the achieved signal level under the assumption of Poisson statistics. This theoretical result can be compared to the experimental value, i.e., the real standard deviation of the same pixels: 1) Fig. 2c (40/40 shots): theoretical rms = 1.4%; 2) Fig. 2c (40/40 shots): experimental rms = 1.3%; 3) Fig. 3a (150/300 shots, averaged over 9 pixels): theoretical rms = 0.2%; and 4) Fig. 3a (150/300 shots, averaged over 9 pixels): experimental rms = 0.2%.

This comparison shows that the measurement precision follows Poisson statistics at least up to a relative error of 0.2%. However, the experiment showed that this limit of 0.2% cannot be improved by higher shot numbers (for example the standard deviation of 0.2% was also obtained in Fig. 3b). Obviously other sources of noise (e.g., electronic read-out errors) become important below this level in the present setup.

Rayleigh Scattering with 248 nm

The KrF laser yields nearly the same scattering intensities as the ArF laser because higher pulse energy is combined with a smaller scattering cross section. It is, however, not only the absolute scattering intensity that counts in the present case, but the limiting noise that is considerably worse for the KrF laser. For example, Mie scattering turned out to be more intense for the KrF laser. Based on a frequency-independent cross section, this is somewhat unexpected. The explanation is probably that the absorption is increased at 193 nm relative to 248 nm. The intense Mie scattering presents problems, particularly for long-time integration over many laser shots, where Mie intensity is summed up in the images as well. For long integration times all images would have to be carefully processed, e.g., by Fourier transform analysis, to remove the high-intensity spots from Mie scattering. In addition to the more intense Mie scattering, the scattered light from background materials increases as well. Consequently Rayleigh scattering at 193 nm is preferred over Rayleigh scattering at 248 nm. In the experiment, Mie scattering from dust particles in the laboratory room air occurred in almost every acquired image, in contrast to the measurements at 193 nm. Figure 5 shows a calibrated image with 100 laser shots at 248 nm (and 200 shots for the calibration image). Some spots from dust particles can be seen in the right half, near the model surface, and a whole trace of a particle that was illuminated many times crosses the warm air stream of the fan in the left half. However, the measurement precision in particle-free areas is comparable to the results at 193 nm.

Results of the Raman Scattering Experiments

Despite the inherent weakness of Raman scattering (roughly 1000 times less than Rayleigh) it presents an attractive alternative to Rayleigh scattering in cases where Mie or surface scattering is too intense, i.e., where the measurement precision is limited by the presence of particles (e.g., condensation in wind tunnels or other particulates). In contrast to Rayleigh scattering, the emission from Raman scattering can be filtered spectrally, very easily and very efficiently, to suppress Mie and surface scattering. Also, in contrast to the Rayleigh measurements, the Raman measurements can be summed over many more laser shots because the interfering emissions can be reduced much more efficiently.

A combination of filters was used to transmit only the vibrational Raman bands of the air components (N_2, O_2, and H_2O) excited by 248-nm laser light, as described in the Experimental section.

A raw image showing planar Raman scattering is given in Fig. 6a. The 400 laser shots were summed in this measurement. The shape of the front end of the model wing (angles $\ell = c = 0$ deg) can be seen in the lower right half of the figure. The surface of the model wing is marked by some remaining stray light (which is not completely rejected by the filter), but this region is very small compared with the Rayleigh scattering measurements due to the eight orders of magnitude attenuation of the rejection filter. This implies that Raman scattering can be observed much closer to the surface (about 1–2 mm) than Rayleigh scattering even at large an-

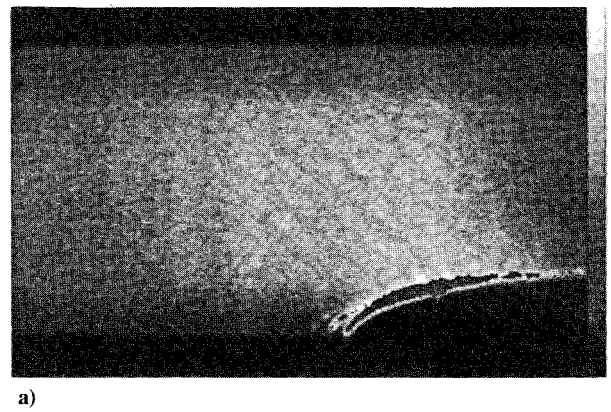

a)

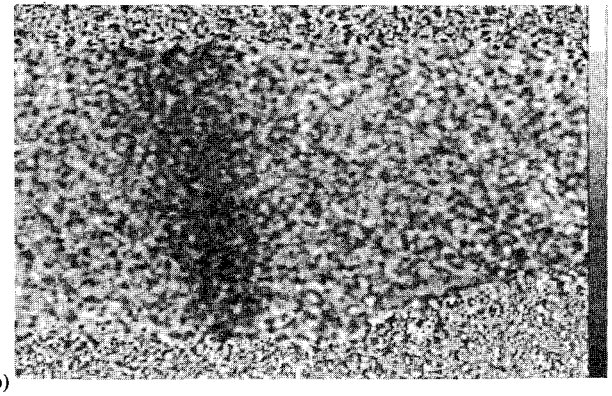

b)

Fig. 6 Spontaneous Raman scattered light a) with the laser sheet illuminating the front end of the model wing; b) is the calibrated result from raw image a).

gles of incidence ℓ. An experiment showed that even an angle of $c = 15$ deg of the surface with respect to the camera axis allowed meaningful measurements, which had to be avoided using Rayleigh scattering.

The detected signal level was a factor of about 560 smaller than it was in the case of Rayleigh scattering at 248 nm. It turned out that the noise level followed Poisson statistics, as was the case with Rayleigh scattering. Hence, the shot numbers had to be increased by a factor of about 560 to achieve the same measurement accuracy as in the Rayleigh scattering experiments.

Figure 6b gives an example of a measurement using 2000 laser shots with the fan turned on divided by an image from 4000 integrated pulses with the fan turned off. Averaging over nine neighboring pixels results in a measurement precision (i.e., a standard deviation of neighboring pixels that were illuminated homogeneously) of: Fig. 6b (2000/4000 shots, averaged over 9 pixels): experimental rms = 1.5%. So the density difference induced by the fan of <= 5.4% can be seen clearly and corresponds nicely to the temperature measured with the thermocouple.

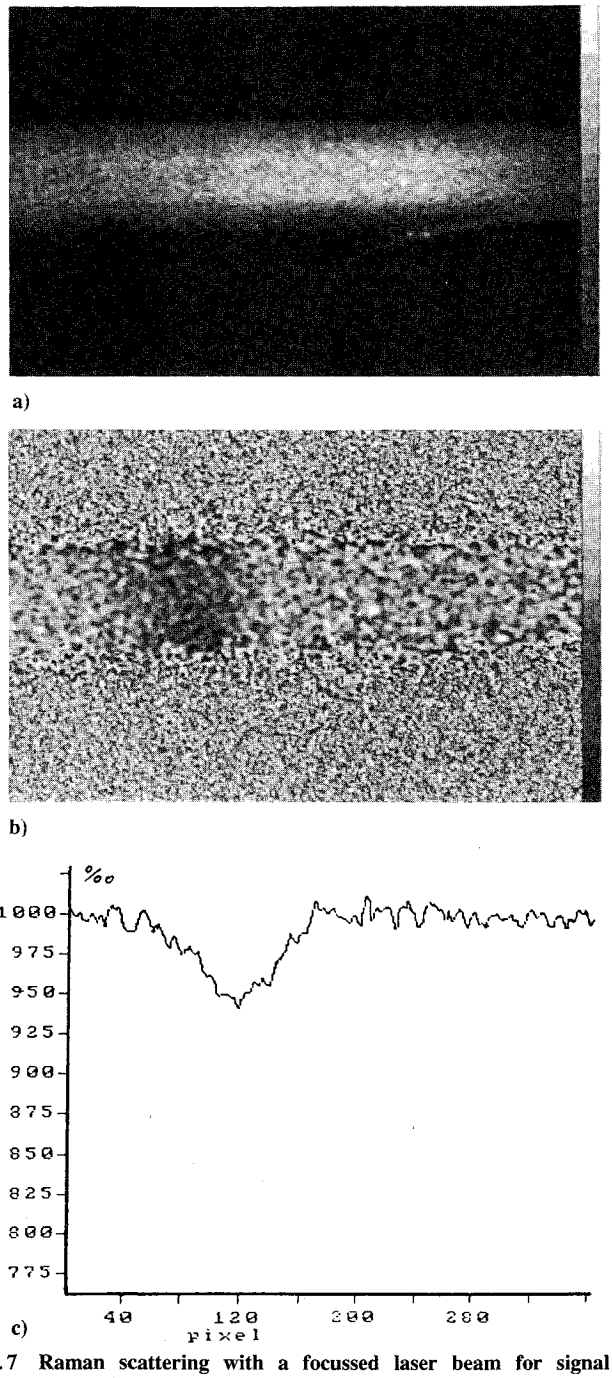

Fig. 7 Raman scattering with a focussed laser beam for signal enhancement: a) raw image and b) calibrated result; and c) the plot is a horizontal profile calculated from b) by averaging over the whole vertical extension of the laser beam.

To increase the accuracy (without changing the laser source, imaging optics, higher shot numbers, or further pixel averaging) the laser light flux can be increased by focusing. Figure 7a shows a situation in which the laser sheet was focused by a factor of 2.4. It turned out that illuminating the surface at large angles of incidence should be avoided with this increased light flux because Raman scattering interferes with some emission in a zone several millimeters wide over the surface, probably arising from photochemical processes on the surface. From an experiment using a spectrograph it is known that broadband emission occurs in the spectral region of the detected Raman lines (258–273 nm) if the focused laser beam is directed onto a metallic surface. This interfering emission cannot be easily discriminated with the technique of E-vector rotation because it is not independent of the E-vector direction. (However, the interfering emission under each Raman band could be subtracted by linear interpolation of the spectral profile if an optical multichannel analyzer, i.e., a spectrograph in combination with a CCD camera, is used. But this would only yield one-dimensional spatial resolution.[8]) It is expected that these emissions will not occur in pure nitrogen (as is the case in some wind tunnels), which is known from experiments using infrared lasers.

To avoid these emissions the laser beam only touched the model wing in the adjustment shown in Fig. 7a. A calibrated image achieved from 1000 laser shots (and 3000 laser shots for the calibration image) is given in Fig. 7b. Averaging over nine neighboring pixels results in a standard deviation of 1.4%.

Further focusing of the laser beam can be simulated (for vertical density structures in the air) by software averaging over a number of pixels in each column. This is done for nearly all rows (50) in the laser sheet area of Fig. 7b, i.e., the sheet is reduced to a one-dimensional line. Applying this method, a standard deviation (i.e., measurement precision) of 0.9% is achieved. The resulting profile is plotted in Fig. 7c, clearly showing a maximum density difference of about 5% induced by the fan. However, the increase in accuracy due to vertical averaging no longer follows Poisson statistics precisely. Obviously another source of noise is active, which is smaller than 1%. This can be explained by read-out errors of the camera electronics or image-intensifier noise. (The deviation of the limiting error value of 0.2% determined in the Rayleigh scattering experiments is probably due to the fact that the image intensifier of the camera system was operated at a higher gain here.)

It should be noted that for comparable laser shot numbers nearly the same accuracy was achieved using one-dimensional Raman scattering (focused laser together with vertical pixel averaging) as was achieved for the two-dimensional Rayleigh scattering experiments.

Further enhancement of Raman scattering intensities with the same shot numbers could be achieved with a larger collection solid angle of the imaging optics. Moreover, a factor of about five could be achieved using a more powerful broadband excimer laser. So it would seem that it is also possible to obtain an accuracy of about 1% (without pixel averaging) in two-dimensional Raman imaging measurements using a few hundred laser shots.

Summary and Conclusions

Variations in air density of less than 1% are measured quantitatively in a plane of 3×6 cm^2 in about 1 s under the extreme condition in which the laser directly irradiates the metal surface of the wing. The signal-to-noise ratio is shown to be determined by photon statistics down to the subpercent level. No effort was made to further increase measurement precision by longer integration times because it is limited by errors in the camera electronics in the subpercent region anyway. In the close vicinity of the wing (about 2–10 mm, depending on the angles with regard to the laser and camera), the strong interference by scattered laser light prevented quantification of the data.

The interference with scattered laser light depends strongly on the angles c and ℓ of the model wing relative to the observation direction and the laser beam. In particular, angles c of more than a few degrees should be avoided. The zone closer to the surfaces

may be analyzed by a modified measurement method using polarization and multiple read-out techniques. The calibration in the homogeneous air has to be performed immediately before or after the actual measurement to make sure that the laser beam has the same position relative to the wing and camera. Also, the E vector of the laser must be aligned perpendicular to the direction of observation to optimize the signal. Rotation of the E vector can be used to generate a reference image for even better discrimination against scattered light. The occurrence of Mie scattering from dust (or condensation in wind tunnels) sets an upper limit for the integration time because the intense single spots from Mie scattering may cover an extended area. Surprisingly, the interference with Mie scattering turned out to be more severe with the KrF laser than with the ArF laser, making the ArF laser more suitable for applications.

The technique of planar Raman scattering was investigated as well, because this technique is much less affected by surface and Mie scattering. This may be of great importance in wind tunnels where condensation may yield strong Mie scattering. It is shown that quantitative measurements can be performed with Raman scattering as well and that these measurements can be made closer to the surface of the wing. The precision of the planar Raman measurements was 5% for 200 and 2% for 1000 laser shots. Longer integration times did not yield improved measurement precision because of some additonal errors, probably arising from the camera. Some possible improvements (detection solid angle, etc.) of the planar Raman technique are believed to yield a measurement precision comparable to that achieved in the Rayleigh scattering experiments.

References

[1]Smith, M., Smits, A., and Miles, R., "Compressible Boundary Layer Density Cross Sections by UV-Rayleigh Scattering," *Optics Letters,* Vol. 14, 1989, pp. 916–918.

[2]Shirinzadeh, B., Balla, J. R., Hillard, M. E., Anders, J. B., Exton, R. J., and Waiting, J. A., "Planar Rayleigh Scattering Results in Helium/Air Mixing Experiments in a Mach 6 Wind Tunnel," *Applied Optics,* Vol. 31, No. 30, 1992, pp. 6529–6534.

[3]Yip, B., and Long, M. B., "Instantaneous Planar Measurement of the Complete Three-Dimensional Scalar Gradient in a Turbulent Jet," *Optics Letters,* Vol. 11, No. 2, 1986, pp. 64–66.

[4]Herzberg, G., "Molecular Spectra and Molecular Structure, I. Spectra of Diatomic Molecules," Krieger Publishing, Malabar, FL, 1950, pp. 446–447.

[5]McKenzie, R. L., "Progress in Laser Spectroscopic Techniques for Aerodynamic Measurements: An Overview," *AIAA Journal,* Vol. 31, No. 3, 1993, pp. 465–477.

[6]Miles, R., and Lempert, L., "Two-Dimensional Measurement of Density, Velocity and Temperature in Turbulent High Speed Air Flows by UV Rayleigh Scattering," *Applied Physics B,* Vol. 51, 1990, pp. 1–7.

[7]McKenzie, R. L., "Rayleigh Rejection Filters for 193 nm ArF laser Raman spectroscopy," *Optics Letters* (submitted for publication).

[8]Grünefeld, G., Beushausen, V., and Andresen, P., "Spatially Resolved Raman Scattering for Multi-Species and Temperature Analysis in Technically Applied Combustion Systems: Spray Flame and Four-Cylinder In-Line Engine," *Applied Physics B* (accepted for publication).